Published OnlineFirst June 26, 2013; DOI: 10.1158/1535-7163.MCT-13-0075

Molecular Cancer Therapeutics

S49076 Is a Novel Kinase Inhibitor of MET, AXL, and FGFR with Strong Preclinical Activity Alone and in Association with Bevacizumab

Mike F. Burbridge, Céline J. Bossard, Carine Saunier, et al.

Mol Cancer Ther 2013;12:1749-1762. Published OnlineFirst June 26, 2013.

Published OnlineFirst June 26, 2013; DOI: 10.1158/1535-7163.MCT-13-0075

Small Molecule Therapeutics

Molecular Cancer Therapeutics

S49076 Is a Novel Kinase Inhibitor of MET, AXL, and FGFR with Strong Preclinical Activity Alone and in Association with Bevacizumab

Mike F. Burbridge[1], Céline J. Bossard[1], Carine Saunier[1], Imre Fejes[5], Alain Bruno[1], Stéphane Léonce[1], Gilles Ferry[2], Georges Da Violante[6], François Bouzom[7], Valérie Cattan[1], Anne Jacquet-Bescond[1], Paolo M. Comoglio[8], Brian P. Lockhart[3], Jean A. Boutin[2], Alex Cordi[4], Jean-Claude Ortuno[4], Alain Pierré[1], John A. Hickman[1], Francisco H. Cruzalegui[1], and Stéphane Depil[1]

Abstract

Aberrant activity of the receptor tyrosine kinases MET, AXL, and FGFR1/2/3 has been associated with tumor progression in a wide variety of human malignancies, notably in instances of primary or acquired resistance to existing or emerging anticancer therapies. This study describes the preclinical characterization of S49076, a novel, potent inhibitor of MET, AXL/MER, and FGFR1/2/3. S49076 potently blocked cellular phosphorylation of MET, AXL, and FGFRs and inhibited downstream signaling *in vitro* and *in vivo*. In cell models, S49076 inhibited the proliferation of MET- and FGFR2-dependent gastric cancer cells, blocked MET-driven migration of lung carcinoma cells, and inhibited colony formation of hepatocarcinoma cells expressing FGFR1/2 and AXL. In tumor xenograft models, a good pharmacokinetic/pharmacodynamic relationship for MET and FGFR2 inhibition following oral administration of S49076 was established and correlated well with impact on tumor growth. MET, AXL, and the FGFRs have all been implicated in resistance to VEGF/VEGFR inhibitors such as bevacizumab. Accordingly, combination of S49076 with bevacizumab in colon carcinoma xenograft models led to near total inhibition of tumor growth. Moreover, S49076 alone caused tumor growth arrest in bevacizumab-resistant tumors. On the basis of these preclinical studies showing a favorable and novel pharmacologic profile of S49076, a phase I study is currently underway in patients with advanced solid tumors. *Mol Cancer Ther; 12(9); 1749–62. ©2013 AACR.*

Introduction

Receptor tyrosine kinases (RTK) bind extracellular ligands to elicit cascades of recruitment and phosphorylation of downstream signaling proteins. Aberrant activity of certain RTKs has been associated with tumor progression in a wide variety of human malignancies, making them promising drug targets for cancer therapy (1).

MET is the RTK for hepatocyte growth factor (HGF). HGF binding induces recruitment of the adaptor protein GAB1 and activation of multiple signaling networks including the phosphoinositide 3-kinase (PI3K)-AKT-mTOR and RAS-RAF-MEK-ERK pathways (2). Collectively, these signals lead to promotion of cell survival, proliferation, migration, invasion and angiogenesis. Deregulation of MET signaling due to overexpression of MET or HGF has been associated with poor prognosis in a wide variety of human malignancies. Activating mutations in MET have been identified in some tumors, directly implicating MET in tumorigenesis (3).

AXL is a member of the TAM family of RTKs, which also includes MER and TYRO-3. Interaction with growth arrest-specific gene 6 (GAS6) activates the PI3K-AKT-mTOR and RAS-RAF-MEK-ERK pathways to promote proliferation, survival, and migration of cancer cells *in vitro* (4) and tumor angiogenesis and metastasis *in vivo* (5). AXL and MER also regulate tumor–stromal cell interactions via secretion of proinflammatory cytokines (6). No activating mutations in AXL have been described, making overexpression of AXL and/or GAS6 the primary mechanisms of activation in a wide range of human cancers in which expression levels often correlate with poor prognosis (6).

The fibroblast growth factor receptors (FGFR) signal essentially via the adaptor protein FRS2 and the PI3K-AKT-mTOR and RAS-RAF-MEK-ERK pathways to

Authors' Affiliations: [1]Oncology Research and Development Unit, [2]Biotechnologies and Molecular and Cellular Pharmacology, [3]Molecular Pharmacology and Pathophysiology, and [4]Medicinal Chemistry, Institut de Recherches Servier, Croissy-sur-Seine, France; [5]Servier Research Institute of Medicinal Chemistry, Budapest, Hungary; [6]Biopharmaceutical Research and [7]Non-Clinical Pharmacokinetics, Technologie Servier, Orléans, France; and [8]Institute for Cancer Research and Treatment, Turin, Italy

Note: Supplementary data for this article are available at Molecular Cancer Therapeutics Online (http://mct.aacrjournals.org/).

Corresponding Author: Mike F. Burbridge, Oncology Research and Development Unit, Institut de Recherches Servier, 125 chemin de Ronde, 78290 Croissy-sur-Seine, France. Phone: 33 155 722 287; E-mail: mike.burbridge@fr.netgrs.com

doi: 10.1158/1535-7163.MCT-13-0075

Published OnlineFirst June 26, 2013; DOI: 10.1158/1535-7163.MCT-13-0075

regulate cellular proliferation, survival, migration, and differentiation. FGFR signaling is not only important for tumor angiogenesis but is also directly implicated in the pathogenesis of a large range of tumor types. Activation of FGFRs is due to abnormal expression levels of the FGFRs or their ligands, mutations, and amplifications (7).

Recently, two important concepts concerning the implication of MET, AXL/MER, the FGFRs, and other RTKs in cancer pathology have emerged. First, not only do these receptors directly or indirectly interact at the cell surface, but also downstream signaling networks may coordinately promote tumor progression. For example, in basal-like breast cancers, MET was shown to interact with, and promote signal transduction downstream of, AXL (8). Increased expression and coactivation of MET and AXL has been described in non–small cell lung cancer (NSCLC; ref. 9) and in mesothelioma (10). MET, the FGFRs, and their respective ligands have been shown to be coexpressed and to synergize in endometrial cancer (11), multiple myeloma (12), and acute myelogenous leukemia (AML; ref. 13). In both NSCLC (14, 15) and gastric cancer (16), functional crosstalk exists between MET or AXL with the HER family members, EGFR and HER3.

Second, studies in recent years have clearly shown a major role of MET, AXL, and FGFRs in primary or acquired resistance to diverse anticancer therapies. For example, amplification of the *MET* gene is seen in up to 20% of EGFR-mutant NSCLC tumors with acquired resistance to EGFR inhibitors (17). Increased MET expression may also confer resistance to EGFR inhibition in colorectal cancer (18). In glioblastomas, MET is proposed to play a key role in resistance to EGFR inhibition (19), VEGF antagonism (20), chemotherapy (21), and radiotherapy (22, 23). Other cancers where aberrant activation of MET may play a role in resistance include bortezomib-resistant multiple myeloma (24), androgen-ablation resistant prostate cancer (25) and chemotherapy-resistant osteosarcoma (26), and pancreatic cancer (27). AXL overexpression and/or activation have been implicated in resistance to cisplatin in ovarian cancer (28) and resistance to imatinib in chronic myelogenous leukemia and in gastrointestinal tumors (29, 30). Cancers where the FGFRs and their ligands have been implicated in resistance mechanisms include resistance to tamoxifen and HER2 inhibitors in breast cancer (31, 32) and to MET inhibition in gastric carcinoma (33).

Importantly, a growing number of cancers are being identified in which all of MET, AXL, and FGFRs have been shown to play a role in resistance mechanisms–either independently or in unison. In the case of EGFR inhibitor–resistant NSCLC, apart from the MET amplification cited above, a recent study also shows a role of AXL in the resistance of approximately 20% of tumors (34). Activation of FGFR2 and FGFR3 has also been documented in NSCLC cell lines treated with EGFR inhibitors (35). MET, AXL, and FGFRs have all been implicated in the resistance of BRAFV600E-mutated melanoma to BRAF inhibitors (36–38) and in chemotherapy-resistant AML (13, 39). Both MET and AXL have been shown to play a role in HER2-positive breast cancer resistant to lapatinib (40, 41) and, in preclinical models, resistance to AKT inhibition (42). Finally, MET, AXL/MER, and FGFRs are important in angiogenesis (3, 5, 7) and as such may confer primary or acquired resistance to inhibitors of VEGF receptor (VEGFR).

Herein, we describe the pharmacologic properties of S49076, a novel, potent ATP-competitive tyrosine kinase inhibitor of MET, AXL/MER, and FGFR1/2/3 currently in phase I clinical trials. S49076 inhibits autophosphorylation of these RTKs and their downstream signaling *in vitro* and *in vivo*, blocks growth and migration of MET-, AXL- and FGFR-overexpressing cells in culture, and shows marked antitumor activity in MET- and FGFR-dependent tumor xenografts at well-tolerated doses.

Materials and Methods

In vitro kinase binding and activity assays

The binding mode of S49076 in the ATP pocket of MET was inferred from X-ray resolution of cocrystal complexes of analogs of S49076 with a C-terminal portion of MET (aa1038-1346; NM_000245.2). The kinetics of interaction of S49076 with MET were studied using real-time label-free interaction analysis. A C-terminal fragment of MET (aa956-1390; NM_000245.2) was captured by its His6 tag on a NTA chip (Biacore) at pH 7.4 at 25°C in 10 mmol/L HEPES, 150 mmol/L NaCl, 0.05% P20, 50 μmol/L EDTA, and 5% dimethyl sulfoxide (DMSO). GluR2 was used as control protein on the reference flow cell. A typical analysis cycle consisted of 200 seconds of MET capture (5 μL/min), followed by 90 seconds sample injection (30 μL/min), 600 seconds of buffer flow (dissociation phase), and then 180 seconds EDTA 350 mmol/L injection to regenerate the flow cell. The kinase-binding selectivity of S49076 was determined on the KINOME*scan* panel of 442 human wild-type and mutated kinases (DiscoveRx). Radiometric biochemical assays for inhibition of AXL, MER, and wild-type and mutated isoforms of MET and FGF receptors were conducted at Millipore.

Cell lines, reagents, and treatments

RT-112 cells were from Cell Lines Service GmbH. GTL-16 cells were from the Institute for Cancer Research and Treatment (IRCC; Turin, Italy). Hepatic cell lines were obtained from the Health Science Research Resources Bank, Japan: HLE (JCRB0404) cells were deposited by J. Sato (Division of Pathology, Cancer Institute, Okayama University Medical School, Okayama, Japan); JHH-2 (JCRB1028), JHH-4 (JCRB0435), and JHH-6 (JCRB1030) cells were deposited by S. Nagamori (Department of Virology II, National Institute of Infectious Diseases, Shinjyuku-ku, Tokyo, Japan). All other cancer cell lines were from the American Type Culture Collection. All cell lines were authenticated by the suppliers (morphology and STR analysis) and were used within 6 months of receipt or resuscitation. MDA-MB-231 cells were cultured

Published OnlineFirst June 26, 2013; DOI: 10.1158/1535-7163.MCT-13-0075

in Eagle's Minimum Essential Medium (EMEM) and all other cells in RPMI-1640. Both media contained 2 mmol/L glutamine and 10% fetal calf serum (FCS). Human umbilical vein endothelial cells (HUVEC) were from PromoCell and cultured in PromoCell growth medium. These cells were authenticated by PromoCell (morphology, immunohistochemical tests for endothelial cell markers). All cells were maintained in a humidified incubator at 37°C with 5% CO_2. Western blots indicating the relative expression and activation levels in these cell lines of the proteins relevant to the current studies are shown in Supplementary Fig. S1.

The hydrochloride salt of S49076 was synthesized at the Servier Research Institute of Medicinal Chemistry in accordance with patent WO2011015728 A1. Nintedanib was purchased from Selleck Chemicals. Bevacizumab was purchased from Roche. For use in cell culture experiments, compounds were dissolved in DMSO at 10 mmol/L and aliquoted at −20°C. siRNAs against AXL and MER were from Qiagen. Nontargeting siRNA and siRNA against TYRO3 were from Dharmacon. Recombinant human growth factors were HGF (R&D Systems 294-HGN), FGF2 (R&D Systems 233-FB/CF), GAS6 (R&D Systems 885-GS), EGF (Sigma E9644), and VEGF ($VEGFA_{165}$, R&D Systems 293-VE/CF).

Antibodies from Cell Signaling Technology were: anti-P(Y1234/1235)MET (#3129), anti-GAB1 (#3232), anti-P(Y627)GAB1 (#3231), anti-AKT (#9272), anti-P(S473)AKT (#9271), anti-P(Y653/654)FGFR (#3471), anti-ERK1/2 (#9102), anti-P(T202/Y204)ERK1/2 (#9101), anti-AXL (#4939), anti-P(702)AXL (#5724), anti-P(Y436)FRS2 (#3861), and anti-MER (#9178); Antibodies from Santa Cruz were: anti-MET (sc-10), anti-FGFR1 (sc-121), anti-FGFR2 (sc-122), anti-FGFR3 (sc-13121), and anti-TYRO3 (sc-1095). Anti-actin was from Millipore (MAB1501R). Anti-FRS2 antibody was from R&D Systems (AF4069). Peroxidase-conjugated secondary antibodies were from Cell Signaling Technology (anti-mouse #7076 and anti-rabbit #7074) and from Santa Cruz Biotechnology (anti-sheep sc-2473).

Protein extracts from cells and xenografts were prepared at 4°C in radioimmunoprecipitation assay extraction buffer (150 mol/L NaCl, 20 mmol/L Tris-HCl pH 7.4, 1% triton X-100, 1 mol/L EGTA, and 1 mmol/L EDTA) to which protease (1% v/v; 539134; Calbiochem) and phosphatase (1% v/v; 524625; Calbiochem) inhibitor cocktails were added. Protein concentration was determined with BCA Protein Assay Kit (Pierce).

To prepare protein extracts from S49076 and nintedanib-treated cells, subconfluent cells were starved in appropriate media containing 0.1% FCS for 24 hours followed by 2 hours of treatment then direct cell lysis in the culture vessels. In siRNA experiments, siRNA duplexes (30 nmol/L) were transfected at 48 hours before cell lysis using 0.15% Lipofectamine 2000 Transfection Reagent (Invitrogen) in complete culture medium. In all experiments where exogenous growth factors were used, cells were treated in the final 10 to 20 minutes before lysis with 20 ng/mL HGF, 50 ng/mL FGF2, 400 ng/mL GAS6, 80 ng/mL EGF, or 30 ng/mL VEGF.

Western blotting and ELISA

For immunoprecipitation of FGFR3, 700 μg of protein extract in 700 μL lysis buffer was incubated with anti-FGFR3 for 2 hours. Fifty microliters of protein A/G agarose (Santa Cruz Biotechnology) was added to the mixture which was incubated on a rotating device for 1 hour. The pellet was collected by centrifugation at 10,000 × *g* for 1 minute and washed four times with lysis buffer. Extracts and immunoprecipitated proteins were diluted into Laemmli sample buffer (Bio-Rad) containing 5% v/v β-mercaptoethanol, or NuPage LDS with reducing agent (Invitrogen), heated for 5 minutes at 95°C, and resolved on Tris-glycine gels or NuPage Bis-Tris gels (Novex; Invitrogen). Biotinylated molecular weight standards (Cell Signaling Technology) were included in all gels. Proteins were transferred to nitrocellulose membranes (Hybond, ECL; Amersham), which were blocked in PBS/0.1% Tween 20 (PBST) containing 5% milk, and probed at 4°C overnight with primary antibodies. Antibodies directed against phosphorylated epitopes were diluted in 5% bovine serum albumin; all other antibodies were diluted in 5% milk. Peroxidase-conjugated secondary antibodies were diluted into 5% milk and applied to membranes for 1 hour at 20°C. Chemiluminescence detection was conducted using the ECL Plus Western Blotting Detection Kit (Amersham) and was recorded on ECL plus hyperfilm (Amersham). Blots were scanned using the Bio-Rad GS-800 calibrated densitometer and quantitative analysis of Western blots was conducted using TotalLab software (Amersham).

Evaluation of P(Y1349)MET, P(Y1054)VEGFR2, P(S473)AKT, P(T421/S424)p70S6K, and corresponding total proteins was conducted according to Meso Scale Discovery ELISA protocols using the Sector Imager 2400 plate reader. The phosphorylation of AXL was evaluated by ELISA at Proqinase in extracts of murine embryonic fibroblasts (MEF) engineered to express a high level of full-length human AXL. When required, IC_{50} values for inhibition of phosphorylated proteins normalized to total proteins were calculated from dose–response curves (XLfit).

Cell viability, migration, and colony formation assays

For GTL-16 and SNU-16 viability assays, cells were seeded in 96-well microplates at the appropriate density in media containing 10% FCS and supplemented 48 hours later with serial dilutions of S49076 in a final volume of 150 μL per well. After 96 hours (GTL-16) or 120 hours (SNU-16) incubation (corresponding to 4 doubling times), 15 μL of a solution of 5 mg/mL MTT (Sigma) was added to each well and the plates were incubated for 4 hours at 37°C. The formazan metabolite was solubilized in SDS for SNU-16 and, following removal of the MTT solution, in DMSO for GTL-16. Global cell viability was estimated by measurement of optical density at 540 nm. Viability assay using MKN-7 cells was conducted at Oncotest (Germany) using a modified propidium iodide (PI) assay. Briefly, cells were

Published OnlineFirst June 26, 2013; DOI: 10.1158/1535-7163.MCT-13-0075

seeded in 96-well microplates at the appropriate density in media containing 10% FCS and supplemented 24 hours later with serial dilutions of S49076 in a final volume of 100 μL per well. After 96 hours, 200 μL of a solution of 7 μg/mL PI was added to each well and the plates were incubated for 2 hours at 20°C. Global cell viability was estimated by measurement of fluorescence on a microplate reader (excitation $\lambda = 530$ nm, emission $\lambda = 620$ nm).

Migration assays were conducted using A549 cells seeded in 96-well microplates and incubated for 24 hours to obtain confluent cultures. One millimeter gaps were introduced by scraping with a pipette tip and cultures were incubated for a further 40 hours with 80 ng/mL HGF and serial dilutions of S49076. The width of the gap was measured using the BD Pathway high-content cell analyzer. Colony formation assays were conducted at Oncotest. Briefly, 5–10 $\times$ 10^3 cells were seeded in agar in 24-well dishes and cultured for 8 to 18 days in Iscove's modified Dulbecco's medium supplemented with 40 ng/mL HGF, 20% FCS, and serial dilutions of S49076. Twenty-four hours before evaluation, vital colonies were stained with 2-(4-iodophenyl)-3-(4-nitrophenyl)-5-phenyltetrazolium chloride. Colonies were counted with an automatic image analysis system (BIOREADER 5000 PRO-XI, Biosys GmbH). Cell lysates were provided by Oncotest for Western blot analyses. IC_{50} values for inhibition of cell viability, migration, or colony formation were calculated from dose–response curves (XLfit).

Mouse studies

Female balb/c and swiss nu/nu mice (Charles River) were used in accordance with institutional guidelines as well as with national and European laws and regulations as put forth by the French Forest and Agriculture Ministry and the standards required by the United Kingdom Coordinating Committee on Cancer Research (43). Mouse weights were more than 18 g at the start of experiments. Doses are expressed as milligrams of free base per kilogram of body weight.

The hydrochloride salt of S49076 was administered orally to mice in 1% (w/v) hydroxyethylcellulose in ammonium acetate buffer pH 4.5 in a volume of 200 μL per 20 g body weight. The maximal tolerated dose of S49076 in these mice was determined to be 100 mg/kg/d (5 days a week for at least 3 weeks). Bevacizumab was dissolved in PBS and administered intraperitoneally in a volume of 200 μL per 20 g body weight.

For pharmacodynamics studies, female nude balb/c nu/nu mice were subcutaneously injected with 10^7 GTL-16 or 5 $\times$ 10^6 SNU-16 cells. When tumors reached a size of approximately 150 mm^3, mice were randomized into homogeneous groups of 3 and given a single oral administration of S49076 at doses of 0.78 to 50 mg/kg. At 2, 6, and 16 hours posttreatment, treated and control mice were sacrificed, tumors were excised, and proteins were extracted in tissue lysis buffer for analysis by Western blot or ELISA. The tumor and blood concentrations of S49076 in tumor-bearing or healthy mice were determined by liquid chromatography/tandem mass spectrometry (LC/MS-MS) analysis of tumor lysates or in blood collected by cardiac puncture into tubes containing EDTA as anticoagulant. For efficacy studies, female nude balb/c nu/nu mice were injected subcutaneously with 10^7 GTL-16 cells, 5 $\times$ 10^6 SNU-16 cells or 10^6 U87-MG cells (the U87-MG cells were first suspended in reconstituted basement membrane, Matrigel, BD Biosciences). When tumors reached a size of approximately 150 mm^3, mice were randomized into homogeneous groups of 8 and treated orally with S49076 at doses of 3.125 to 100 mg/kg once or twice daily for 5 days a week for up to 4 weeks.

Studies of S49076 in association with bevacizumab were carried out using swiss nu/nu mice injected subcutaneously with 10^7 HT-29 or LS-174T cells. In the HT-29 study, when tumors reached a size of approximately 150 mm^3, mice were randomized into homogeneous groups of 10 and treated orally with S49076 (50 or 100 mg/kg) once daily for 5 days a week for 3 weeks and/or intraperitoneally with bevacizumab (10 mg/kg) twice weekly for 3 weeks. In the LS-174T study, when tumors reached a size of approximately 100 mm^3, mice were randomized, 12 mice were maintained untreated, and the remainder were treated intraperitoneally with bevacizumab twice weekly for 2 weeks. Two weeks later, bevacizumab-treated mice were further split into 3 groups of 10 mice and treated or not with 50 mg/kg S49076 orally twice daily 5 days a week for 3 weeks or with 10 mg/kg bevacizumab intraperitoneally twice weekly for 3 weeks. In all studies, antitumor efficacy was monitored by at least twice weekly measurement of tumor sizes using calipers and body weights were recorded to document potential general toxicity. Percentage tumor growth inhibition on a given day was calculated using the formula: [1-RTV (treated)/RTV(untreated)] $\times$ 100, where RTV = relative tumor volume on the given day versus start of treatment. Statistical analyses were conducted using two-way ANOVA with repeated measures over time followed by Dunnett test on log tumor volumes.

Body weight loss was less than 5% for all groups, all time points, and in all experiments.

Results

S49076 is a potent inhibitor of wild-type and mutated isoforms of MET, AXL, MER, and FGFR1/2/3

S49076 was discovered through medicinal chemistry supported by structural biology and molecular modeling to identify potent and selective MET inhibitors. The binding mode of S49076 in the ATP pocket of MET was inferred from X-ray resolution of cocrystal complexes of analogs of S49076 with the C-terminal portion of MET (Fig. 1). Real-time label-free interaction analysis of S49076 with the C-terminal portion of MET enabled determination of on-rate (k_a, 1.27 $\times$ 10^6 $M^{-1}s^{-1}$), off-rate (k_d, 1.62 $\times$ 10^{-3} s^{-1}), and dissociation constant (K_D, 1.26 $\times$ 10^{-9} mol/L). In radiometric assays, S49076 potently inhibited the tyrosine

Published OnlineFirst June 26, 2013; DOI: 10.1158/1535-7163.MCT-13-0075

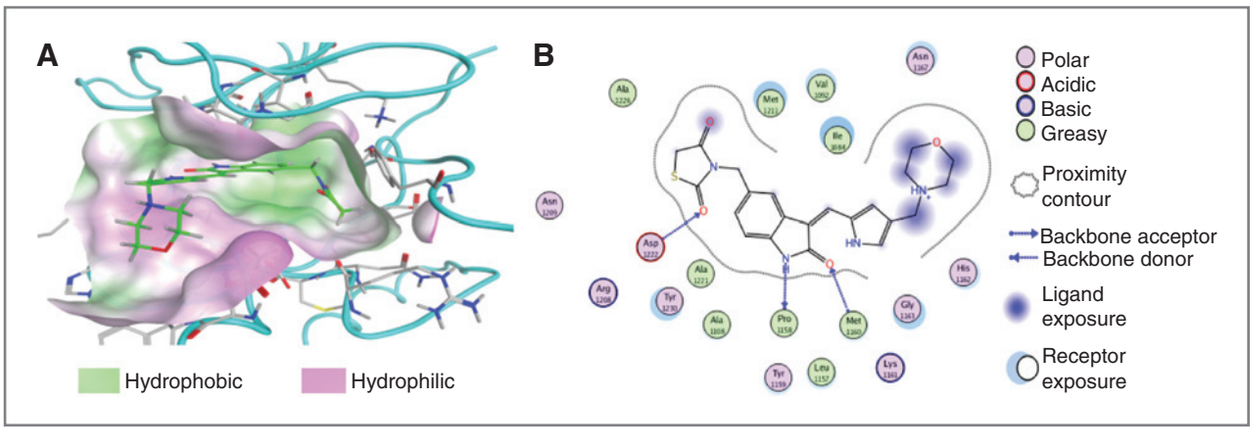

Figure 1. S49076, 3-[(3-{[4-(4-Morpholinylméthyl)-1H-pyrrol-2-yl]méthylène}-2-oxo-2,3-dihydro-1H-indol-5-yl)méthyl]-1,3-thiazolidine-2,4-dione, is a MET ATP-pocket binder. A, the binding mode of S49076 in the ATP pocket of MET inferred from X-ray resolution of cocrystal complexes of analogs of S49076 with the C-terminal portion of MET. B, schematic illustration of the binding mode showing two interactions in the hinge region between the oxindole moiety and Pro1158 / Met1160 and a third interaction between a carbonyl group of the thiazolidinedione and the N-H backbone of Asp1222.

kinase activity of MET, AXL, MER, and FGFR1/2/3 with IC_{50} values below 20 nmol/L. Importantly, S49076 also inhibited the kinase activity of all tested clinically relevant mutated isoforms of MET and FGFR1/2 at similar concentrations (Table 1). The kinase-binding selectivity of S49076 was determined on a panel of 442 human wild-type and mutated kinases. At 100 nmol/L, apart from the primary targets MET, AXL/MER, and FGFRs, only 6% of kinases were identified as hits. The kinase interaction map for S49076 is shown in Supplementary Fig. S2.

Table 1. IC_{50} values for the inhibition by S49076 of MET, AXL, MER, and FGFR1/2/3 in radiometric assays

Kinase	Examples of tumors where these mutations have been detected	IC_{50} (nmol/L)
MET	—	1
MET^{D1246N}	Germline renal papillary carcinoma	8
MET^{Y1248C}		16
MET^{D1246H}	Somatic papillary renal cell carcinoma, head and neck squamous cell carcinoma, non-small-cell lung carcinoma	11
MET^{Y1248D}		17
MET^{Y1248H}		1
MET^{M1268T}		1
AXL	—	7
MER	—	2
FGFR1	—	18
$FGFR1^{V561M}$	Squamous cell lung cancer	23
FGFR2	—	17
$FGFR2^{N549H}$	Endometrial carcinoma	19
FGFR3	—	15

S49076 selectively inhibits MET, AXL, and FGFR1/2/3 signaling in cancer cells

The capacity of S49076 to inhibit MET, AXL, and FGFR1/2/3 activation and signaling was evaluated in cancer cells in which these RTKs were either constitutively active or activated by addition of their respective ligand. The autophosphorylation of MET at tyrosines Tyr1234/1235 in the C-terminal cytoplasmic domain was evaluated by Western blot analysis in H441 NSCLC cells in which MET is overexpressed and constitutively active. Total inhibition of MET phosphorylation was seen after 2 hours of incubation with 10 nmol/L S49076 and an IC_{50} of 2 nmol/L was calculated from densitometric analysis. Signal transduction downstream of MET is largely mediated by the adaptor protein GAB1 which is phosphorylated by MET on Tyr627 (3). Corresponding inhibition of GAB1 phosphorylation on this site by S49076 was also seen (Fig. 2A). The autophosphorylation of MET on tyrosine Tyr1349 in the C-terminal cytoplasmic domain is critical for recruitment and activation of signal transduction molecules and adaptor proteins (3). S49076 inhibited MET phosphorylation on this site in GTL-16 gastric carcinoma cells with an IC_{50} value of 3 nmol/L and IC_{90} value of 10 nmol/L as evaluated by ELISA (Fig. 2B).

The inhibition of AXL phosphorylation by S49076 was evaluated by ELISA in MEFs expressing human AXL. The IC_{50} for AXL inhibition by S49076 was 56 nmol/L (Fig. 2C). Activation of AXL following binding to GAS6 leads to signal transduction via the phosphorylation on Ser473 of AKT (2). However, GAS6 also binds and activates the two other receptors of the TAM family, MER and TYRO3. To evaluate the specific inhibition of AXL signaling in cancer cells by S49076, it was necessary to identify cells in which the activation of AKT by GAS6 depended exclusively on AXL. To this end, we used siRNA technology to knock down AXL, MER, and TYRO3 separately or in combination with MDA-MB-231 breast cancer cells followed by addition of GAS6 and evaluation of AKT phosphorylation

Published OnlineFirst June 26, 2013; DOI: 10.1158/1535-7163.MCT-13-0075

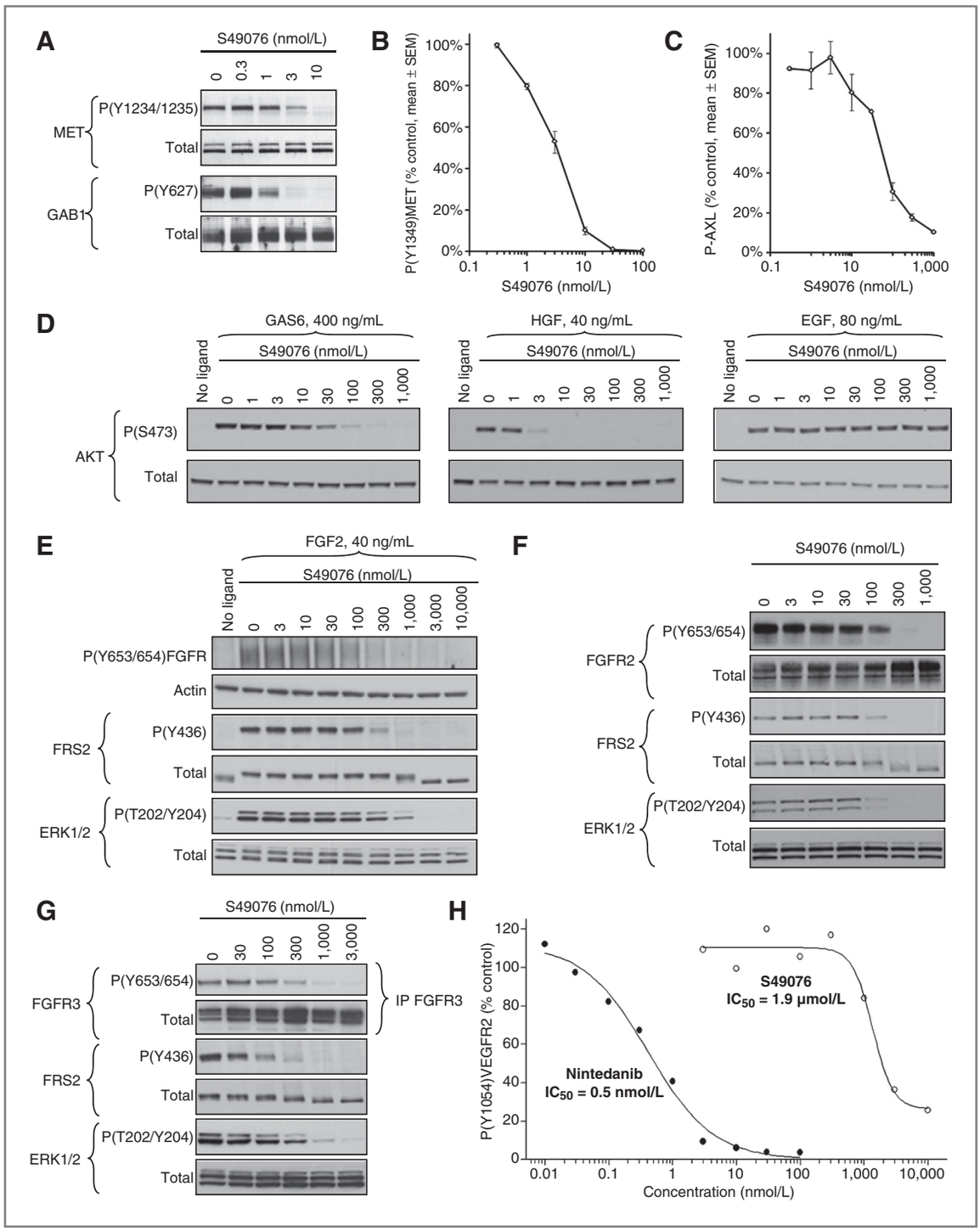

Figure 2. S49076 selectively inhibits MET, AXL, and FGFR1/2/3 signaling in cancer cells following 2-hour incubation at the indicated concentrations. A, inhibition of MET and GAB1 phosphorylation in H441 cells. Western blots using antibodies to phosphorylated and total proteins from one representative experiment are shown. Densitometric analysis of the blots indicated IC_{50}s of 2 and 1 nmol/L for the inhibition of MET and GAB1 phosphorylation respectively. B, inhibition of MET phosphorylation in GTL-16 cells. Levels of phosphorylated and total MET were evaluated by ELISA. Data are from four independent experiments in which levels of phosphorylated MET were normalized to total protein. S49076 inhibited MET phosphorylation with an IC_{50} of 3 nmol/L and an IC_{90} of 10 nmol/L. C, inhibition of AXL phosphorylation in murine embryonic fibroblasts engineered to express human AXL. Level of phosphorylated AXL was evaluated by ELISA. Data (mean ± SD) are from duplicate wells. S49076 inhibited AXL phosphorylation with an IC_{50} of 56 nmol/L. D, inhibition of AKT phosphorylation in MDA-MB-231 cells. GAS6, HGF, or EGF were added at the indicated concentrations for the final 10 to 20 minutes before lysis. Western blots using antibodies to phosphorylated and total proteins from one representative experiment are shown. (*Continued on the following page.*)

Published OnlineFirst June 26, 2013; DOI: 10.1158/1535-7163.MCT-13-0075

by Western blot analysis. In these cells, while AXL knockdown completely ablated AKT phosphorylation following GAS6 addition, knockdown of MER and/or TYRO3 had no effect (Supplementary Fig. S3). It was thus considered that AXL was the major driver of AKT phosphorylation. In this model, S49076 inhibited AXL signaling via AKT with an IC_{50} of 33 nmol/L (Fig. 2D). To further show the selectivity of S49076 for MET and AXL signaling, MDA-MB-231 cells treated with S49076 were stimulated with HGF to activate MET, or EGF to activate EGFR. As expected, AKT phosphorylation was inhibited in the low nanomolar range in the presence of HGF, whereas no inhibition was seen at up to 1 μmol/L in the presence of EGF (Fig. 2D).

The inhibition of FGFR1/2/3 and their downstream signaling was evaluated in cancer cells known to individually overexpress each of these receptors. The H1703 NSCLC cell line has high levels of FGFR1 (44) which was activated by addition of FGF2. The SNU-16 gastric and RT-112 bladder cancer cell lines overexpress constitutively active forms of FGFR2 and FGFR3, respectively (45, 46). In these cells, S49076 inhibited the autophosphorylation of the receptors on Tyr653/654 and the phosphorylation of the FGFR-specific adaptor protein FRS2 on Tyr436. Densitometric analyses allowed calculation of IC_{50} values which were in all cases between 50 and 200 nmol/L. Corresponding decreases in phosphorylation of the downstream signaling proteins ERK1/2 on Thr202/Tyr204 was also seen (Fig. 2E–G).

Many multitarget kinase inhibitors currently in clinical development potently inhibit VEGFR2. Although this receptor is implicated in tumor angiogenesis, it also has an important physiologic role in the maintenance of vascular tone and its inhibition may dictate the maximum tolerated dose for these molecules (47). VEGFR2 was not among the kinases bound by S49076 in the kinase profile. However, to confirm lack of potent inhibition of this kinase in a cellular context, the intracellular autophosphorylation of VEGFR2 at Tyr1054 was evaluated by ELISA after incubation of HUVECs with S49076, followed by stimulation with VEGF. The IC_{50} was 1.9 μmol/L for S49076 and 0.5 nmol/L for nintedanib, a dual VEGFR-FGFR inhibitor used as positive control (Fig. 2H).

S49076 inhibits viability, motility, and three-dimensional colony formation of cancer cells expressing MET, AXL, or FGFRs

GTL-16 cells are dependent on overexpressed, constitutively active MET for proliferation (2), whereas the viability of SNU-16 cells depends on amplified, constitutively active, FGFR2 (45). S49076 inhibited the viability of each of these cell lines in monolayer culture with IC_{50} values of 3 and 167 nmol/L, respectively. In GTL-16 cells, the IC_{90} for inhibition of viability was 5 nmol/L (Fig. 3A). At this concentration, the inhibition of MET phosphorylation on Tyr1349 was 65% (Fig. 2B), suggesting that partial inhibition of MET was sufficient for near-maximal effect on growth. A third human gastric carcinoma cell line, MKN-7, reported to be dependent on EGFR activity for survival and proliferation in monolayer culture (48), was insensitive to S49076 at concentrations of up to 10 μmol/L, thus confirming the target selectivity of S49076. The ability of S49076 to inhibit MET-driven migration was evaluated using the A549 human NSCLC cell line in which migration was induced by addition of HGF. S49076 potently inhibited migration in this model with an IC_{50} of 14 nmol/L (Fig. 3B).

Preclinical and clinical studies suggest that the principal roles of AXL may be in migration and metastasis rather than in proliferation and survival of cells of the primary tumor (5). One model which may reflect the capacity of tumor cells to survive and grow independently of anchorage to an extracellular matrix is the soft agar colony formation assay. Screening of a large number of cell lines by Western blot analysis enabled the identification of three hepatocarcinoma cell lines in which AXL was highly expressed and activated (Supplementary Fig. S1B). S49076 potently inhibited the three-dimensional growth in soft agar of these cells, whereas no effect was seen on a fourth hepatocarcinoma cell line in which AXL was expressed and activated at much lower levels (Fig. 3C). All four cell lines did, however, also express both FGFR1 and FGFR2 and displayed phosphorylation of FRS2 (Supplementary Fig. S1), so it is possible that this effect on clonogenic survival was partially due to inhibition of FGFRs. Interestingly, none of these cell lines were sensitive to S49076 in a monolayer culture, possibly confirming a major role of AXL in anchorage-independent growth.

S49076 inhibits MET and FGFR2 phosphorylation as well as tumor growth in MET- and FGFR2-dependent xenografts at doses predicted from cell assays and pharmacokinetic studies

The capacity of S49076 to inhibit MET signaling was evaluated in subcutaneous GTL-16 xenografts. Following oral administration at subtoxic doses, S49076 inhibited the phosphorylation of MET at Tyr1349 in a dose- and time- dependent manner (Fig. 4A). Inhibition was

(*Continued.*) Densitometric analysis of the blots indicated an IC_{50} of 33 nmol/L for the inhibition of AKT phosphorylation following activation of AXL signaling by GAS6. E to G, inhibition of FGFR1, FGFR2, and FGFR3 phosphorylation by S49076 in H1703 (E), SNU-16 (F), and RT-112 (G) cells, respectively, and corresponding inhibition of phosphorylation of FRS2 and ERK1/2. FGF2 was added for the final 10 minutes before lysis in the case of the H1703 cells (E). Western blots using antibodies to phosphorylated and total proteins from one representative experiment in each case are shown. FGFR3 in the RT-112 cells (G) was immunoprecipitated before Western blot analysis. Densitometric analysis of the blots indicated IC_{50}s of 68, 95, and 200 nmol/L, respectively, for the inhibition of the phosphorylation of FGFR1, FGFR2, and FGFR3. H, S49076 does not potently inhibit VEGFR2 in HUVECs. VEGF was added for the final 10 minutes before lysis. Phosphorylation of VEGFR2 was evaluated by ELISA. Data are from a representative experiment. The IC_{50}s were 1.9 μmol/L for S49076 and 0.5 nmol/L for nintedanib.

Published OnlineFirst June 26, 2013; DOI: 10.1158/1535-7163.MCT-13-0075

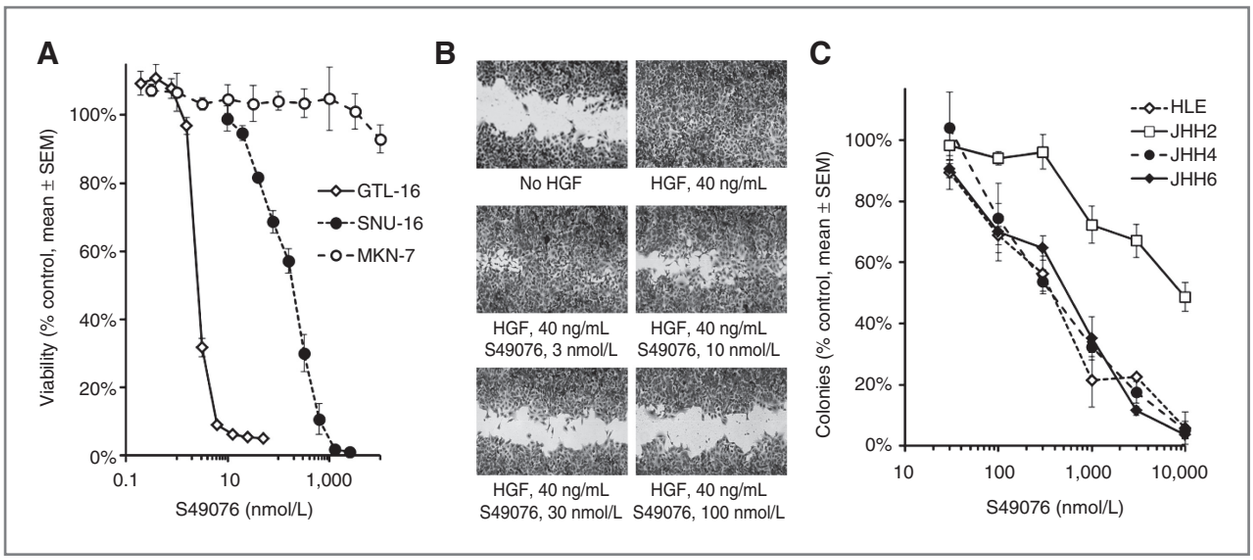

Figure 3. S49076 inhibits viability, motility, and three-dimensional colony formation of cancer cells expressing MET, AXL, or FGFRs. A, inhibition of viability of GTL-16, SNU-16, and MKN-7 cells. Cells were incubated for 4 doubling times in the presence of a range of concentrations of S49076. Viability was measured by MTT (GTL-16 and SNU-16) or PI (MKN-7) assay. IC_{50} values were 3, 167, and >10 μmol/L for GTL-16, SNU-16, and MKN-7, respectively. B, inhibition of motility in A549 cells. A gap was made in confluent cell monolayers which were then incubated for 40 hours in the presence of HGF and a range of concentrations of S49076. Image analysis enabled calculation of an IC_{50} for inhibition of cell motility of 14 nmol/L. C, inhibition of colony formation of HLE, JHH2, JHH4, and JHH6 cells in soft agar. Cultures were incubated for 8 to 18 days in a range of concentrations of S49076. Colonies were visualized and counted with an automatic image analysis system.

more than 80% for all doses from 3.125 mg/kg at 2 and 6 hours posttreatment. At 6.25 mg/kg, inhibition of MET phosphorylation was 95% and 58% at 6 and 16 hours posttreatment, respectively. We previously showed that chronic inhibition of MET in GTL-16 cells led to attenuation of the phosphorylation of proximal and distal transducers of the RAS pathway, including AKT and p70S6K (2). At 6 hours postadministration, a dose-dependent inhibition of the phosphorylation of these signaling proteins was observed (Fig. 4B). The relationship between dose of S49076 and blood levels is shown in Fig. 4C and D. Apparent saturated absorption and possibly saturated elimination occurred at 100 mg/kg where blood concentration at 2 hours was 7 μmol/L. Numerical pharmacokinetic data is provided in Supplementary Table S1. For near-complete P(Tyr1349)MET inhibition at 2 hours, a dose of 3.125 mg/kg corresponding to a blood concentration of 100 nmol/L was required. Given that the free-fraction of S49076 is estimated to be 20%, this corresponded to approximately 20 nmol/L free compound. This is in agreement with the *in vitro* evaluation of MET phosphorylation in GTL-16 cells where 10 nmol/L was required for 90% inhibition (Fig. 2B). Interestingly, the inhibition of P(Tyr1349)MET at 6 hours for all doses was similar to that at 2 hours. This could be explained by high distribution of S49076 to the tumors, in which the half-life for the dose of 3.125 mg/kg was approximately 7 hours versus less than 2 hours in the blood. Hence, at this dose, the intratumor concentration of S49076 remained above 100 nmol/L for at least 16 hours following treatment (Fig. 4E).

Cell assays using GTL-16 cells suggested that 65% inhibition of P(Tyr1349)MET was required for a 90% inhibition of tumor cell viability (Figs. 2B and 3A). Taking into account the inhibition at 16 hours, a minimum daily dose of between 6.25 mg/kg and 12.5 mg/kg would therefore be expected to lead to around 90% inhibition of tumor growth in this xenograft model. At the end of the four-week treatment period, inhibition of tumor growth was 69%, 82%, 91%, 95%, and 103% for the doses of 3.125, 6.25, 12.5, 25, and 50 mg/kg, respectively (Fig. 5A). This corresponds to between 41% and 91% inhibition of MET phosphorylation at the 16-hour time point in the primary pharmacodynamics study (Figs. 4A and 5C) and agrees with the predictions of the relationship between the *in vitro* inhibition of MET and cell viability. The antitumor activity of S49076 was confirmed in U87-MG human glioblastoma xenografts in which MET is activated by autocrine HGF. At the end of the second week of treatment, inhibition of tumor growth was 90%, 78%, and 103% for the doses of 6.25, 12.5, and 25 mg/kg, respectively, and at 50 mg/kg tumors regressed by 68% (Fig. 5B).

The ability of S49076 to inhibit the *in vivo* phosphorylation of FGFR2 was shown in SNU-16 subcutaneous xenografts. Two hours following administration, inhibition of FGFR2 phosphorylation was 93% at 12.5 mg/kg. This corresponded to 1 μmol/L blood concentration (Fig. 4C) and approximately 200 nmol/L free compound. This is in agreement with the *in vitro* evaluation of FGFR2 phosphorylation in SNU-16 cells where 300 nmol/L was required for complete inhibition (Fig. 2B). To maintain more than 80% inhibition at 6 and at 16 hours, a dose of 50

Published OnlineFirst June 26, 2013; DOI: 10.1158/1535-7163.MCT-13-0075

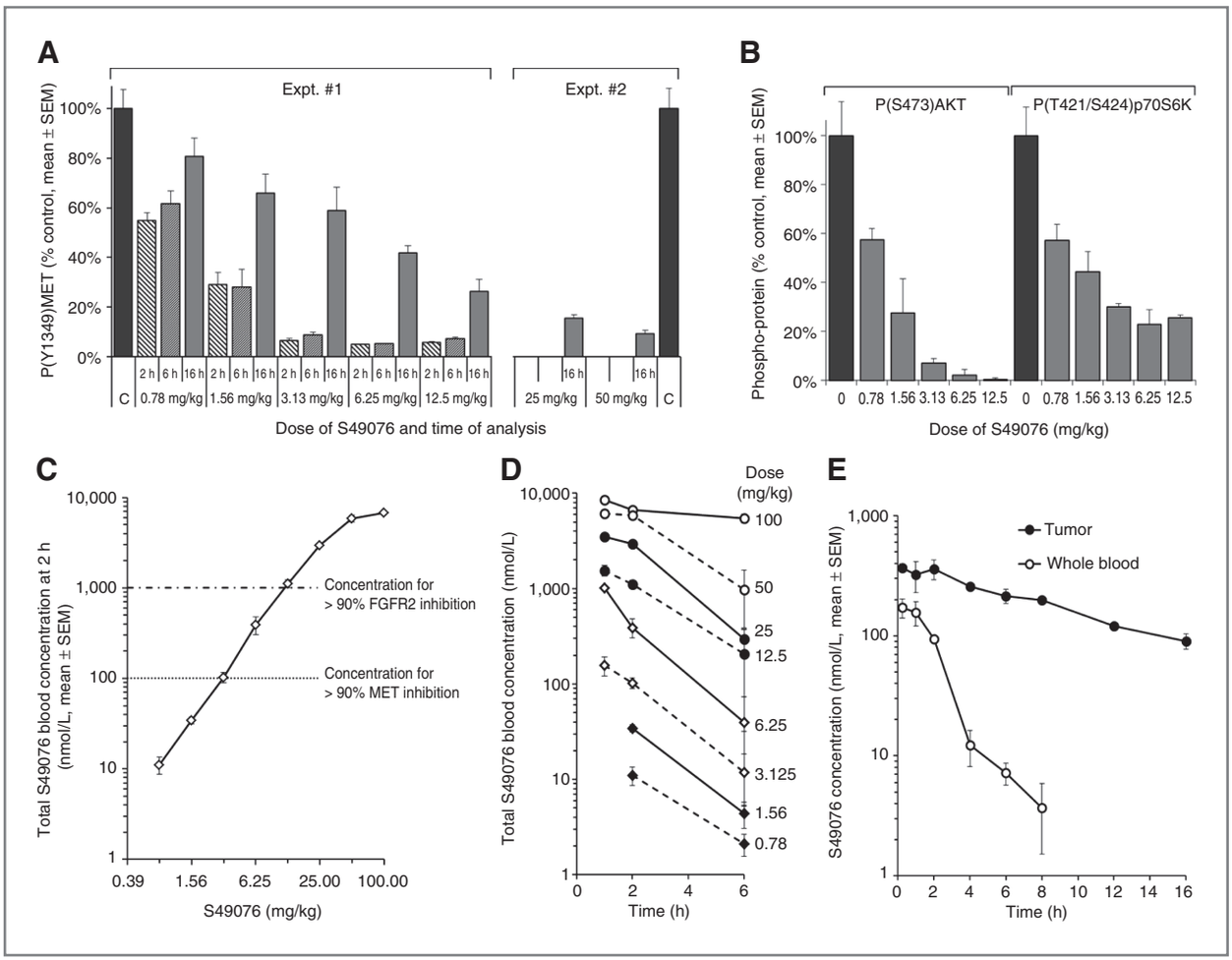

Figure 4. Orally administered S49076 inhibits MET signaling in subcutaneous xenografts in balb/c nu/nu mice at doses predicted from cell assays and pharmacokinetic studies. A and B, inhibition of MET, AKT, and p70S6K phosphorylation in GTL-16 tumors. Following treatment with S49076 at the indicated doses, 3 tumors were excised at each time point, lysed, and MET (A), AKT, and p70S6K (B) phosphorylation was measured by ELISA. Data shown for AKT and p70S6K phosphorylation are for the 6-hour time point. C to E, blood (C, D, E) and tumor (E) concentration of S49076 in healthy mice following S49076 administration, determined by LC/MS-MS analysis. Blood concentration is shown as a function of dose 2 hours following S49076 administration (C) and as a function of time following S49076 administration at a range of doses (D). Blood levels predicted to be necessary for more than 90% inhibition of MET and FGFR phosphorylation are indicated (C). Tumor and blood concentrations are shown as a function of time following administration of 3.125 mg/kg S49076 (E).

mg/kg was required (Fig 5D). The inhibition of FGFR2 signaling was confirmed by the parallel loss of Tyr436 phosphorylation on the FGFR-associated adaptor protein FRS2 (Fig. 5E). Tumor growth inhibition by oral administration of S49076 in these SNU-16 tumors was studied using a once-daily or twice-daily oral treatment schedule. At the end of the treatment period, inhibition of tumor growth was 61%, 91%, and 100% for the once daily doses of 50, 75, and 100 mg/kg, respectively, and 102% and 103% for the twice daily doses of 37.5 and 50 mg/kg, respectively (Fig. 5F).

S49076 is active in a bevacizumab-resistant model and totally inhibits the growth of colon carcinoma xenografts in association with bevacizumab

Bevacizumab is a VEGF antagonist approved in combination for treatment of several diseases including colorectal cancers. However, responses are only partial and of limited duration (49). In subcutaneous HT-29 colon carcinoma xenografts, twice weekly treatment with bevacizumab at 10 mg/kg led to 71% inhibition of tumor growth at the end of treatment (Fig. 6A). HT-29 cells express VEGFR1 and VEGFR3 (50), so this effect may have been due to a combination of effects on the vasculature and the tumor cells themselves. S49076 alone at 100 mg/kg per day also only induced a partial inhibition of 65%. This was to be expected as this tumor was not found to be sensitive to S49076 in either monolayer or three-dimensional soft agar culture. However, combined therapy with bevacizumab and S49076 led to near total arrest of tumor growth. To determine whether tumors with acquired resistance to bevacizumab were sensitive to S49076 a LS-174T xenograft model of colon carcinoma was used in which tumors ceased to respond to bevacizumab within 2 to 3 weeks of

Published OnlineFirst June 26, 2013; DOI: 10.1158/1535-7163.MCT-13-0075

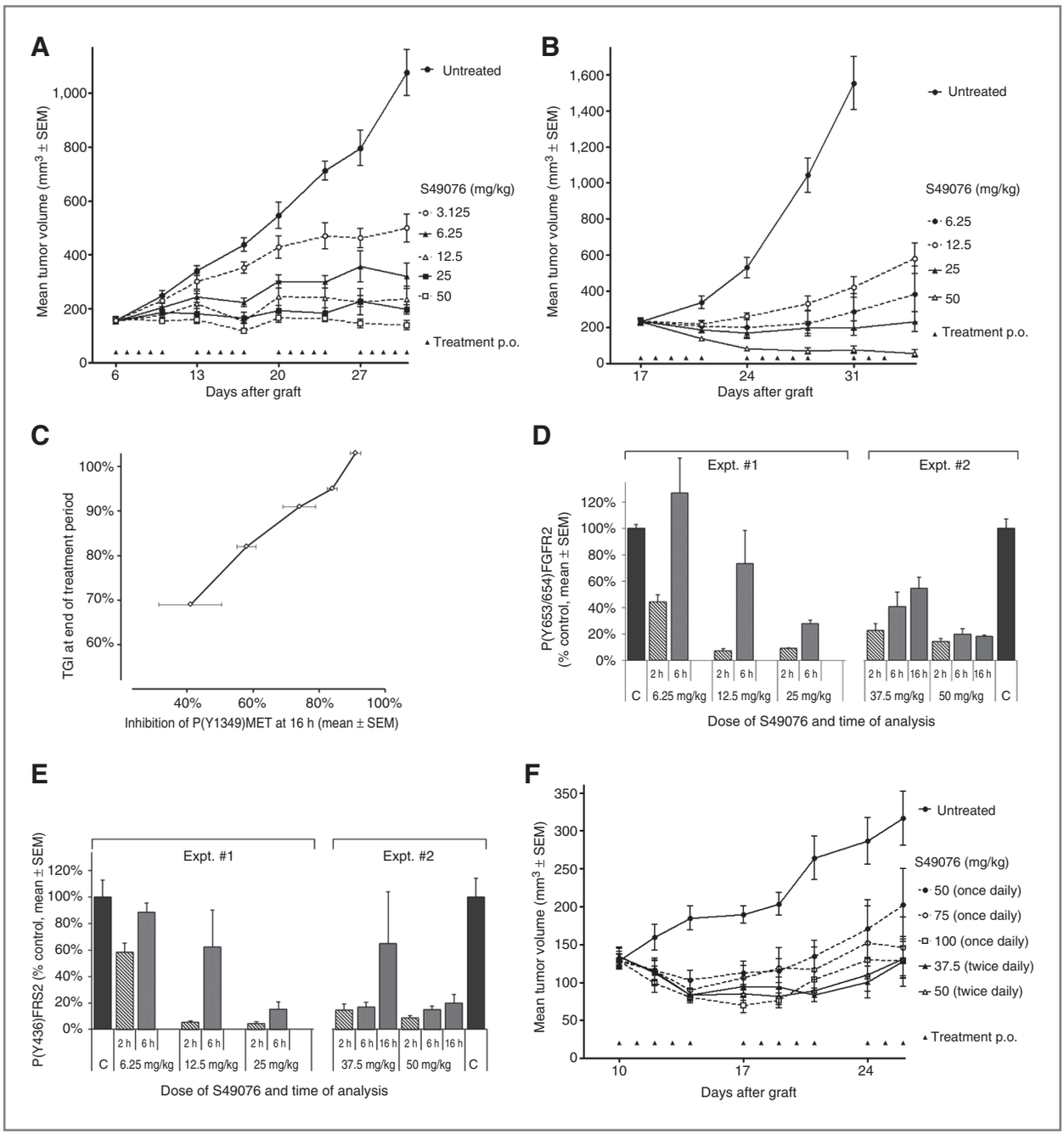

Figure 5. Orally administered S49076 inhibits MET-dependent tumor growth in subcutaneous xenografts in balb/c nu/nu mice at doses predicted from pharmacodynamic studies and inhibits FGFR2 signaling and tumor growth in FGFR2-dependent xenografts. A, inhibition of the growth of GTL-16 tumor xenografts. S49076 was administered at a range of doses once-daily for 5 days a week as indicated. Tumor volumes were significantly less than for control mice (*, $P \leq 0.01$) for the dose of 3.125 mg/kg on days 24 through 31 and at all other doses on days 13 through 31. B, inhibition of the growth of U87-MG tumor xenografts. S49076 was administered at a range of doses once daily for 5 days a week as indicated. Tumor volumes were significantly less than for control mice ($P \leq 0.01$) at all doses on days 17 through 31. C, relationship between inhibition of MET phosphorylation at 16 hours postadministration and tumor growth inhibition (TGI) at the end of the treatment period. D and E, inhibition of FGFR2 and FRS2 phosphorylation in SNU-16 tumors. Following treatment with S49076 at the indicated doses, 3 tumors were excised at each time point, lysed, and FGFR2 (D) and FRS2 (E) phosphorylation was evaluated by densitometric analysis of Western blots. Data are shown for two independent experiments using different dose ranges. F, inhibition of the growth of SNU-16 tumor xenografts. S49076 was administered at a range of doses once daily or twice daily for 5 days a week as indicated. Tumor volumes were significantly less than for control mice ($P \leq 0.01$) for twice daily treatment on days 14 through 26 and for once daily treatment at 75 and 100 mg/kg on days 14, 21, and 26. In the case of once daily treatment at 50 mg/kg, tumor volumes were significantly less than for control mice ($P \leq 0.05$) on days 14 and 21. Statistical analysis was performed using two-way ANOVA with repeated measures over time followed by Dunnett test on log tumor volumes. p.o., *per os*.

Published OnlineFirst June 26, 2013; DOI: 10.1158/1535-7163.MCT-13-0075

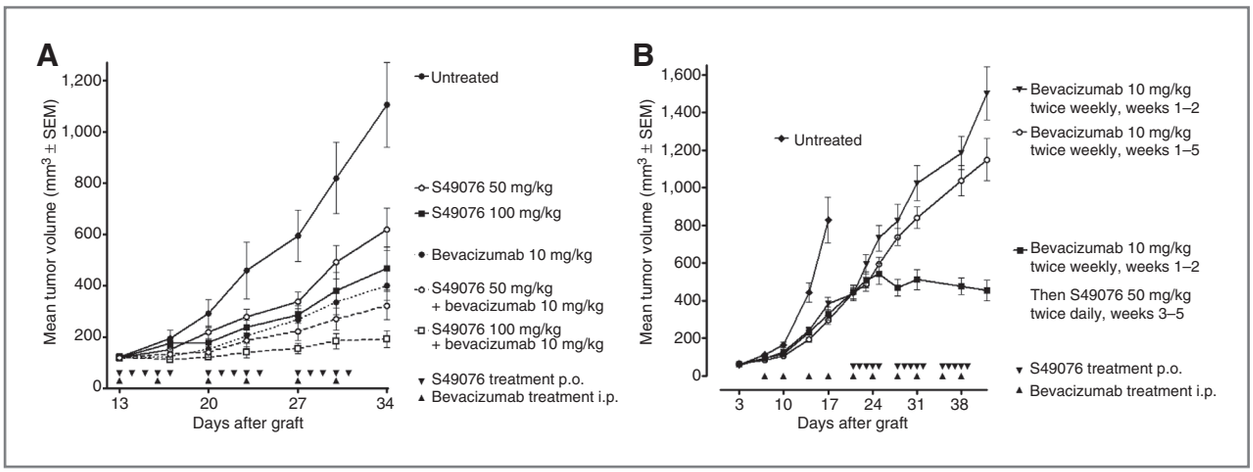

Figure 6. Orally administered S49076 is active in association with bevacizumab and in a bevacizumab-resistant model in swiss nu/nu mice. A, inhibition of the growth of HT-29 tumor xenografts. S49076 was administered at a range of doses once daily for 5 days a week, alone or in association with bevacizumab administered intraperitoneally at 10 mg/kg twice a week. Tumor volumes were significantly less than for control mice ($P \leq 0.01$) for mice treated with 100 mg/kg S49076 alone on days 27 through 34 and for all mice treated with bevacizumab alone or in association with S49076 on days 20 through 34. Tumor volumes in mice treated with bevacizumab in association with 100 mg/kg S49076 were significantly less ($P \leq 0.05$) than those in mice treated with either 100 mg/kg S49076 alone or with bevacizumab alone on days 30 and 34. B, inhibition of the growth of LS-174T tumor xenografts. Mice were treated intraperitoneally (i.p.) with bevacizumab twice weekly for 2 weeks before being split into 3 groups and treated as indicated with S49076 or bevacizumab. Tumor volumes in mice treated continuously (weeks 1–5) with bevacizumab were not significantly different from those in mice treated with bevacizumab for 1 to 2 weeks only. Tumor volumes in mice treated with 10 mg/kg bevacizumab for 1 to 2 weeks followed by 50 mg/kg S49076 for 3 to 5 weeks were significantly less ($P \leq 0.01$) than those in all mice treated with bevacizumab alone on days 28 through 42. Statistical analysis was performed using two-way ANOVA with repeated measures over time followed by Dunnett test on log tumor volumes.

treatment (Fig. 6B). Markedly, in this model, subsequent treatment with S49076 led to complete tumor growth arrest, suggesting a switch from dependency on VEGFR for angiogenesis to a dependency on MET, AXL, or FGFR.

Discussion

MET, AXL, and FGFRs have been associated with tumor progression in a wide variety of human malignancies, where they act individually or in synergy to activate concerted downstream signaling networks. A major emerging role of these RTKs is in cancers where primary or acquired resistance is observed to existing therapies, including those targeting other RTKs. A drug that will simultaneously target MET, AXL, and FGFRs will thus be of potential benefit not only for patients where any one of these receptors is activated individually, but also in those cases where combined inhibition of these RTKs is required for maximal therapeutic efficacy.

Here, we describe the pharmacologic properties of a novel, potent, orally active ATP-competitive tyrosine kinase inhibitor of MET, AXL/MER, and FGFR1/2/3. S49076 inhibited these kinases and clinically relevant mutated isoforms in isolated enzyme assays with IC_{50}s of below 20 nmol/L. Although the clinical incidence of MET mutations in cancer is relatively rare as compared with that seen for the FGFRs, it is possible that mutations in MET may emerge as a mechanism of resistance to certain of the highly selective wild-type MET inhibitors currently in clinical trials (1). In cell assays, S49076 inhibited the autophosphorylation of MET in the low nanomolar range and the autophosphorylation of AXL and FGFR1/2/3 at IC_{50} values of less than 200 nmol/L. Downstream signaling from these receptors via adaptor proteins and through AKT or ERK1/2 was inhibited at similar concentrations. Importantly, unlike many moderately selective or multikinase inhibitors, S49076 is not a potent inhibitor of VEGFR2 in cell assays. Although VEGFR2 is implicated in tumor angiogenesis, it also plays a major physiologic role in the maintenance of vascular tone, and its inhibition by other RTK inhibitors limits dosing of these molecules in the clinic (47).

The target-specific activity of S49076 was further shown in functional cell assays, where S49076 potently reduced the viability in monolayer cultures of both MET- and FGFR2-dependent gastric cancer cells while having no effect on a third gastric cancer cell line reported to be dependent on EGFR. Major roles of MET in cancer progression are the promotion of cell migration, invasion, and metastasis. The potential of S49076 to block MET-driven cancer cell motility was shown by the potent inhibition of the MET-driven migration of lung carcinoma cells. Regarding AXL, no cell line has yet been identified in which this RTK has been shown to have a major role in viability in monolayer culture. Indeed, preclinical and clinical studies suggest that the principal roles of AXL may be in processes linked to metastasis rather than in progression of the primary tumor (5). However, here we show that S49076 potently inhibits the three-dimensional growth in soft agar of hepatocarcinoma cells overexpressing activated forms of AXL and FGFR2, whereas little effect was seen on a hepatocarcinoma cell line in which AXL was expressed at much lower levels. Interestingly,

Published OnlineFirst June 26, 2013; DOI: 10.1158/1535-7163.MCT-13-0075

none of these cell lines was sensitive to S49076 in monolayer culture, indicating a major role of AXL in anchorage-independent growth. Further work will be required to determine the relative importance of AXL and FGFR2 in the survival of these cell lines, although, in light of the published roles of AXL in resistance, it is reasonable to hypothesize that simultaneous inhibition of AXL and FGFR2 may be required for efficacy in these models. Further investigation of the mechanism of action of S49076 in these models is in progress.

In animal pharmacodynamic studies, oral administration of S49076 to nude mice at subtoxic doses led to the inhibition of MET phosphorylation in subcutaneous GTL-16 human gastric carcinoma xenografts in a dose-dependent and time-dependent manner. Inhibition was more than 80% for all doses from 3.125 mg/kg at 2 and 6 hours posttreatment, whereas a dose of 6.25 mg/kg was required to give more than 50% inhibition at 16 hours. Pharmacokinetics in nude mice was linear up to 50 mg/kg, and pharmacokinetic/pharmacodynamic studies showed a good relationship between blood concentrations and inhibition of MET phosphorylation. S49076 was highly distributed to the tumors and at doses of 6.25 mg/kg and higher, more than 50% inhibition of MET phosphorylation was retained at 16 hours. Following chronic once daily treatment in this GTL-16 model, more than 80% tumor growth inhibition by S49076 was observed for the doses of 6.25 mg/kg and higher at the end of treatment. Importantly, the relationship between inhibition of tumor growth and reduction of MET phosphorylation observed in the pharmacodynamics study was in agreement with predictions from cellular assays. Marked tumor growth inhibition was also seen in the subcutaneous U87-MG human glioblastoma model, which displays an HGF-MET autocrine loop. In this model, the tumor regression observed at 50 mg/kg may have been due to additional inhibition of AXL and the FGFRs, possibly via inhibition of angiogenesis, as other MET inhibitors, such as crizotinib, do not cause tumor shrinkage in this model (51). The *in vivo* inhibition of the phosphorylation of FGFR2 by S49076 was shown in SNU-16 gastric tumor xenografts. Two hours following administration, inhibition of FGFR2 phosphorylation was more than 90% at 12.5 mg/kg. In this tumor, to maintain more than 50% inhibition of P-FGFR2 at 6 and 16 hours, a dose of 37.5 mg/kg or more was required. This inhibition of the phosphorylation of FGFR2 was mirrored by a reduction in the phosphorylation of the downstream adaptor protein, FRS2. In this model, dose-dependent inhibition of tumor growth was observed following either once-daily or twice-daily treatment. Together, these studies show robust inhibition of both MET and FGFR at well-tolerated doses giving rise to marked inhibition of tumor growth. On the basis of this data, both once-daily and twice-daily administration schedules are being investigated in the clinic. To date, no xenograft models have been identified where growth of the primary tumor is dependent on the activity of AXL alone. However, the potent inhibition of AXL signaling by S49076 in cell assays at concentrations inferior to those required to inhibit the FGFRs strongly suggest that this target will also be hit in animal models. More complex models where AXL has been implicated in breast tumor metastasis (5) are currently being explored.

Except the rare MET-addicted tumors, one of the major applications of MET inhibitors will likely be in cancers where resistance preexists or has developed against other targeted therapies (1). One such therapy is bevacizumab, which blocks the interaction of VEGF with its receptors, VEGFR1/2/3. Preclinical studies have shown that although continuous VEGF pathway inhibition in endothelial cells of the tumor vasculature will initially slow tumor growth via inhibition of angiogenesis, this will be followed by rapid revascularization and increased tumor invasiveness, most likely due to induction of hypoxic conditions, upregulation of hypoxia-inducible factor 1, and increased expression of proangiogenic genes including MET (49). In addition, MET activity has been shown to regulate the secretion of VEGF by tumor cells (50). Interestingly, VEGFRs may be expressed by tumor cells also, and a recent study using models of glioblastoma has elegantly shown the role of VEGF in the recruitment of the protein tyrosine phosphatase 1B (PTP1B) to a MET/VEGFR2 heterocomplex, thereby suppressing MET autophosphorylation in response to HGF. Thus, although knockout of VEGF in glioblastoma tumors grown intracranially in mice led to prolongation of survival, increased HGF-induced MET phosphorylation was observed. Knockdown of MET in these VEGF-null glioblastoma tumors further extended survival (20). Although it is not yet known whether this interaction between VEGFRs, MET, and PTP1B exists in cancers other than glioblastomas, the coexpression of VEGFR and MET by tumors of various origin makes a similar mechanism of MET activation likely. Together with the implication of MET in angiogenesis, these results clearly identify clinical potential for combined anti-VEGF and anti-MET therapy. The fact that both AXL and the FGFRs also play a role in tumor angiogenesis (5, 7) further reinforces the rationale for combination of anti-VEGF therapy with S49076. This was shown in a subcutaneous model of colon carcinoma, in which both the tumor cells and the endothelial cells are known to express VEGFRs. In this model, combined treatment of S49076 with bevacizumab led to near total inhibition of tumor growth as compared with only partial inhibition by either S49076 or bevacizumab alone. It is possible that this was due to a combination of the effects of VEGFR, MET, AXL, and FGFR inhibition in both the tumor and endothelial cells. In the clinic, responses to bevacizumab are of limited duration (49). In a colon carcinoma model created to recapitulate this acquired resistance to bevacizumab treatment, S49076 led to complete tumor growth arrest, suggesting a switch from dependency on VEGFR for angiogenesis to a dependency on MET, AXL, or FGFR. Together, these models showing preclinical antitumor efficacy in association with bevacizumab and in bevacizumab-resistant tumors suggests

Published OnlineFirst June 26, 2013; DOI: 10.1158/1535-7163.MCT-13-0075

that S49076 may be of benefit in combination with bevacizumab in colorectal cancer treatment in the clinic.

In recent years, a number of studies have shown a major role of not only MET but also AXL/MER and FGFRs in primary or acquired resistance to diverse anticancer therapies, including chemeotherapeutic agents, radiotherapy, and targeted therapies. Indeed, it seems likely that a prominent clinical use of agents targeting these RTKs will be in association with existing or emerging treatments. Furthermore, it is worth noting that an increasing number of cancer types are being identified in which two or more of these RTKs have been reported to play a role in resistance mechanisms, either independently or together. These cancers include EGFR inhibitor-resistant NSCLC (17, 34, 35), BRAF-inhibitor resistant BRAFV600E-mutated melanoma (36–38), and chemotherapy-resistant AML (13, 39) in which all three RTKs have been shown to play a role. Both MET and AXL have been implicated in and lapatinib-resistant HER2-positive breast cancer (40, 41). Taken together, this emerging understanding of clinical resistance mechanisms and the data presented in this report concerning S49076, a novel, potent inhibitor of MET, AXL, and FGFRs, clearly indicate the clinical potential of S49076 either alone or in association with other therapies in a wide range of tumor types. In animal models, blood and tumor levels of S49076 were consistent with robust inhibition of these targets. Importantly, the unique kinase inhibition profile of S49076 may allow inhibition of these oncogenic RTKs without dose limitation due to the side effects related to VEGFR2 inhibition. On the basis of these preclinical studies showing a favorable and novel pharmacologic profile of S49076, a phase I study is currently underway in patients with advanced solid tumors.

Disclosure of Potential Conflicts of Interest

J.A. Hickman is a consultant/advisory board member of Servier and Johnson & Johnson. No potential conflicts of interest were disclosed by the other authors.

Authors' Contributions

Conception and design: M.F. Burbridge, A. Bruno, P. M. Comoglio, A. Cordi, J.A. Hickman, S. Depil
Development of methodology: C.J. Bossard, C. Saunier, A. Bruno, B.P. Lockhart
Acquisition of data (provided animals, acquired and managed patients, provided facilities, etc.): C.J. Bossard, C. Saunier, A. Bruno, B.P. Lockhart, A. Pierre
Analysis and interpretation of data (e.g., statistical analysis, biostatistics, computational analysis): M.F. Burbridge, C.J. Bossard, C. Saunier, I. Fejes, A. Bruno, G. Ferry, G.D. Violante, F. Bouzom, J.-C. Ortuno, A. Pierre, F.H. Cruzalegui
Writing, review, and/or revision of the manuscript: M.F. Burbridge, C.J. Bossard, A. Bruno, G. Ferry, G.D. Violante, V. Cattan, A. Jacquet-Bescond, J.-C. Ortuno, J.A. Hickman, F.H. Cruzalegui, S. Depil
Administrative, technical, or material support (i.e., reporting or organizing data, constructing databases): J.A. Boutin
Study supervision: M.F. Burbridge, A. Bruno, S. Leonce, A. Pierre, J.A. Hickman, F.H. Cruzalegui, S. Depil

Acknowledgments

The authors thank Nolwen Guigal-Stephan and Gaëlle Rolland Valognes for helpful discussion and Pascal Aumond, Thomas Edmonds, Fabienne Gravé, Michel Jan, Gaëlle Lysiak-Auvity, Laetitia Marini, and Emilie Schneider for technical assistance.

The costs of publication of this article were defrayed in part by the payment of page charges. This article must therefore be hereby marked *advertisement* in accordance with 18 U.S.C. Section 1734 solely to indicate this fact.

Received January 30, 2013; revised May 8, 2013; accepted June 10, 2013; published OnlineFirst June 26, 2013.

References

1. Janne PA, Gray N, Settleman J. Factors underlying sensitivity of cancers to small-molecule kinase inhibitors. Nat Rev Drug Discov 2009;8:709–23.
2. Bertotti A, Burbridge MF, Gastaldi S, Galimi F, Torti D, Medico E, et al. Only a subset of Met-activated pathways are required to sustain oncogene addiction. Sci Signal 2009;2:ra80.
3. Trusolino L, Bertotti A, Comoglio PM. MET signalling: principles and functions in development, organ regeneration and cancer. Nat Rev Mol Cell Biol 2010;11:834–48.
4. Paccez JD, Vasques GJ, Correa RG, Vasconcellos JF, Duncan K, Gu X, et al. The receptor tyrosine kinase Axl is an essential regulator of prostate cancer proliferation and tumor growth and represents a new therapeutic target. Oncogene 2013;32:689–98.
5. Li Y, Ye X, Tan C, Hongo JA, Zha J, Liu J, et al. Axl as a potential therapeutic target in cancer: role of Axl in tumor growth, metastasis and angiogenesis. Oncogene 2009;28:3442–55.
6. Verma A, Warner SL, Vankayalapati H, Bearss DJ, Sharma S. Targeting Axl and Mer kinases in cancer. Mol Cancer Ther 2011;10:1763–73.
7. Brooks AN, Kilgour E, Smith PD. Molecular pathways: fibroblast growth factor signaling: a new therapeutic opportunity in cancer. Clin Cancer Res 2012;18:1855–62.
8. Gujral TS, Karp RL, Finski A, Chan M, Schwartz PE, Macbeath G, et al. Profiling phospho-signaling networks in breast cancer using reverse-phase protein arrays. Oncogene 2013;32:3470–6.
9. Rikova K, Guo A, Zeng Q, Possemato A, Yu J, Haack H, et al. Global survey of phosphotyrosine signaling identifies oncogenic kinases in lung cancer. Cell 2007;131:1190–203.
10. Ou WB, Hubert C, Corson JM, Bueno R, Flynn DL, Sugarbaker DJ, et al. Targeted inhibition of multiple receptor tyrosine kinases in mesothelioma. Neoplasia 2011;13:12–22.
11. Felix AS, Edwards RP, Stone RA, Chivukula M, Parwani AV, Bowser R, et al. Associations between hepatocyte growth factor, c-Met, and basic fibroblast growth factor and survival in endometrial cancer patients. Br J Cancer 2012;106:2004–9.
12. Mahtouk K, Moreaux J, Hose D, Reme T, Meissner T, Jourdan M, et al. Growth factors in multiple myeloma: a comprehensive analysis of their expression in tumor cells and bone marrow environment using Affymetrix microarrays. BMC Cancer 2010;10:198.
13. Kentsis A, Reed C, Rice KL, Sanda T, Rodig SJ, Tholouli E, et al. Autocrine activation of the MET receptor tyrosine kinase in acute myeloid leukemia. Nat Med 2012;18:1118–22.
14. Tanizaki J, Okamoto I, Sakai K, Nakagawa K. Differential roles of transphosphorylated EGFR, HER2, HER3, and RET as heterodimerisation partners of MET in lung cancer with MET amplification. Br J Cancer 2011;105:807–13.
15. Gusenbauer S, Vlaicu P, Ullrich A. HGF induces novel EGFR functions involved in resistance formation to tyrosine kinase inhibitors. Oncogene. Epub 2012 Oct 8.
16. Corso S, Ghiso E, Cepero V, Sierra JR, Migliore C, Bertotti A, et al. Activation of HER family members in gastric carcinoma cells mediates resistance to MET inhibition. Mol Cancer 2010;9:121.
17. Turke AB, Zejnullahu K, Wu YL, Song Y, Dias-Santagata D, Lifshits E, et al. Preexistence and clonal selection of MET amplification in EGFR mutant NSCLC. Cancer Cell 2010;17:77–88.

Published OnlineFirst June 26, 2013; DOI: 10.1158/1535-7163.MCT-13-0075

18. Liska D, Chen CT, Bachleitner-Hofmann T, Christensen JG, Weiser MR. HGF rescues colorectal cancer cells from EGFR inhibition via MET activation. Clin Cancer Res 2011;17:472–82.
19. Jun HJ, Acquaviva J, Chi D, Lessard J, Zhu H, Woolfenden S, et al. Acquired MET expression confers resistance to EGFR inhibition in a mouse model of glioblastoma multiforme. Oncogene 2012;31: 3039–50.
20. Lu KV, Chang JP, Parachoniak CA, Pandika MM, Aghi MK, Meyronet D, et al. VEGF inhibits tumor cell invasion and mesenchymal transition through a MET/VEGFR2 complex. Cancer Cell 2012;22:21–35.
21. Chu SH, Ma YB, Feng DF, Zhang H, Qiu JH, Zhu ZA. c-Met antisense oligodeoxynucleotides increase sensitivity of human glioma cells to paclitaxel. Oncol Rep 2010;24:189–94.
22. Lal B, Xia S, Abounader R, Laterra J. Targeting the c-Met pathway potentiates glioblastoma responses to gamma-radiation. Clin Cancer Res 2005;11:4479–86.
23. De Bacco F, Luraghi P, Medico E, Reato G, Girolami F, Perera T, et al. Induction of MET by ionizing radiation and its role in radioresistance and invasive growth of cancer. J Natl Cancer Inst 2011;103:645–61.
24. Que W, Chen J, Chuang M, Jiang D. Knockdown of c-Met enhances sensitivity to bortezomib in human multiple myeloma U266 cells *via* inhibiting Akt/mTOR activity. APMIS 2012;120:195–203.
25. Verras M, Lee J, Xue H, Li TH, Wang Y, Sun Z. The androgen receptor negatively regulates the expression of c-Met: implications for a novel mechanism of prostate cancer progression. Cancer Res 2007;67: 967–75.
26. Wang K, Zhuang Y, Liu C, Li Y. Inhibition of c-Met activation sensitizes osteosarcoma cells to cisplatin *via* suppression of the PI3K-Akt signaling. Arch Biochem Biophys 2012;526:38–43.
27. Shah AN, Summy JM, Zhang J, Park SI, Parikh NU, Gallick GE. Development and characterization of gemcitabine-resistant pancreatic tumor cells. Ann Surg Oncol 2007;14:3629–37.
28. Macleod K, Mullen P, Sewell J, Rabiasz G, Lawrie S, Miller E, et al. Altered ErbB receptor signaling and gene expression in cisplatin-resistant ovarian cancer. Cancer Res 2005;65:6789–800.
29. Dufies M, Jacquel A, Belhacene N, Robert G, Cluzeau T, Luciano F, et al. Mechanisms of AXL overexpression and function in Imatinib-resistant chronic myeloid leukemia cells. Oncotarget 2011;2:874–85.
30. Mahadevan D, Cooke L, Riley C, Swart R, Simons B, Della Croce K, et al. A novel tyrosine kinase switch is a mechanism of imatinib resistance in gastrointestinal stromal tumors. Oncogene 2007;26: 3909–19.
31. Turner N, Pearson A, Sharpe R, Lambros M, Geyer F, Lopez-Garcia MA, et al. FGFR1 amplification drives endocrine therapy resistance and is a therapeutic target in breast cancer. Cancer Res 2010;70: 2085–94.
32. Azuma K, Tsurutani J, Sakai K, Kaneda H, Fujisaka Y, Takeda M, et al. Switching addictions between HER2 and FGFR2 in HER2-positive breast tumor cells: FGFR2 as a potential target for salvage after lapatinib failure. Biochem Biophys Res Commun 2011;407:219–24.
33. Bachleitner-Hofmann T, Sun MY, Chen CT, Liska D, Zeng Z, Viale A, et al. Antitumor activity of SNX-2112, a synthetic heat shock protein-90 inhibitor, in MET-amplified tumor cells with or without resistance to selective MET Inhibition. Clin Cancer Res 2011;17:122–33.
34. Zhang Z, Lee JC, Lin L, Olivas V, Au V, LaFramboise T, et al. Activation of the AXL kinase causes resistance to EGFR-targeted therapy in lung cancer. Nat Genet 2012;44:852–60.
35. Ware KE, Marshall ME, Heasley LR, Marek L, Hinz TK, Hercule P, et al. Rapidly acquired resistance to EGFR tyrosine kinase inhibitors in NSCLC cell lines through de-repression of FGFR2 and FGFR3 expression. PLoS ONE 2010;5:e14117.
36. Straussman R, Morikawa T, Shee K, Barzily-Rokni M, Qian ZR, Du J, et al. Tumour micro-environment elicits innate resistance to RAF inhibitors through HGF secretion. Nature 2012;487:500–4.
37. Johannessen CM, Boehm JS, Kim SY, Thomas SR, Wardwell L, Johnson LA, et al. COT drives resistance to RAF inhibition through MAP kinase pathway reactivation. Nature 2010;468:968–72.
38. Yadav V, Zhang X, Liu J, Estrem S, Li S, Gong XQ, et al. Reactivation of mitogen-activated protein kinase (MAPK) pathway by FGF receptor 3 (FGFR3)/Ras mediates resistance to vemurafenib in human B-RAF V600E mutant melanoma. J Biol Chem 2012;287:28087–98.
39. Hong CC, Lay JD, Huang JS, Cheng AL, Tang JL, Lin MT, et al. Receptor tyrosine kinase AXL is induced by chemotherapy drugs and overexpression of AXL confers drug resistance in acute myeloid leukemia. Cancer Lett 2008;268:314–24.
40. Minuti G, Cappuzzo F, Duchnowska R, Jassem J, Fabi A, O'Brien T, et al. Increased MET and HGF gene copy numbers are associated with trastuzumab failure in HER2-positive metastatic breast cancer. Br J Cancer 2012;107:793–9.
41. Liu L, Greger J, Shi H, Liu Y, Greshock J, Annan R, et al. Novel mechanism of lapatinib resistance in HER2-positive breast tumor cells: activation of AXL. Cancer Res 2009;69:6871–8.
42. Chandarlapaty S, Sawai A, Scaltriti M, Rodrik-Outmezguine V, Grbovic-Huezo O, Serra V, et al. AKT inhibition relieves feedback suppression of receptor tyrosine kinase expression and activity. Cancer Cell 2011;19:58–71.
43. Workman P, Twentyman P, Balkwill F, Balmain A, Chaplin D, Double J, et al. United Kingdom Co-ordinating Committee on Cancer Research (UKCCCR) guidelines for the Welfare of Animals in Experimental Neoplasia (Second Edition). Br J Cancer 1998;77:1–10.
44. Marek L, Ware KE, Fritzsche A, Hercule P, Helton WR, Smith JE, et al. Fibroblast growth factor (FGF) and FGF receptor-mediated autocrine signaling in non-small-cell lung cancer cells. Mol Pharmacol 2009;75:196–207.
45. Kunii K, Davis L, Gorenstein J, Hatch H, Yashiro M, Di Bacco A, et al. FGFR2-amplified gastric cancer cell lines require FGFR2 and Erbb3 signaling for growth and survival. Cancer Res 2008;68:2340–8.
46. Gomez-Roman JJ, Saenz P, Molina M, Cuevas Gonzalez J, Escuredo K, Santa Cruz S, et al. Fibroblast growth factor receptor 3 is overexpressed in urinary tract carcinomas and modulates the neoplastic cell growth. Clin Cancer Res 2005;11:459–65.
47. Chen HX, Cleck JN. Adverse effects of anticancer agents that target the VEGF pathway. Nat Rev Clin Oncol 2009;6:465–77.
48. Motoyama AB, Hynes NE, Lane HA. The efficacy of ErbB receptor-targeted anticancer therapeutics is influenced by the availability of epidermal growth factor-related peptides. Cancer Res 2002;62: 3151–8.
49. Grepin R, Pages G. Molecular mechanisms of resistance to tumour anti-angiogenic strategies. J Oncol 2010;2010:835680.
50. Morelli MP, Brown AM, Pitts TM, Tentler JJ, Ciardiello F, Ryan A, et al. Targeting vascular endothelial growth factor receptor-1 and -3 with cediranib (AZD2171): effects on migration and invasion of gastrointestinal cancer cell lines. Mol Cancer Ther 2009;8:2546–58.
51. Zou HY, Li Q, Lee JH, Arango ME, McDonnell SR, Yamazaki S, et al. An orally available small-molecule inhibitor of c-Met, PF-2341066, exhibits cytoreductive antitumor efficacy through antiproliferative and antiangiogenic mechanisms. Cancer Res 2007; 67:4408–17.